

Original Article



OPEN ACCESS

Received: Oct 27, 2024

Revised: Mar 7, 2025

Accepted: Mar 12, 2025

Published online: Apr 9, 2025

*Correspondence to

Nattiya Hirankarn

Center of Excellence in Immunology and Immune Mediated Diseases, Department of Microbiology, Faculty of Medicine, Chulalongkorn University, 1873 Rama IV Rd, Pathum Wan, Bangkok 10330, Thailand.
Email: nattiya.h@chula.ac.th

Kornvalee Meesilpavikkai

Department of Microbiology, Faculty of Medicine, Chulalongkorn University, 1873 Rama IV Rd, Pathum Wan, Bangkok 10330, Thailand.
Email: kornvalee.m@chula.ac.th

Copyright © 2025. The Korean Association of Immunologists

This is an Open Access article distributed under the terms of the Creative Commons Attribution Non-Commercial License (<https://creativecommons.org/licenses/by-nc/4.0/>) which permits unrestricted non-commercial use, distribution, and reproduction in any medium, provided the original work is properly cited.

ORCID iDs

Kornvalee Meesilpavikkai <https://orcid.org/0000-0002-3502-6345>
Kasiphak Kaikaew <https://orcid.org/0000-0002-1790-1839>
Zijun Zhou <https://orcid.org/0000-0001-8761-7828>
Virgil A.S.H. Dalm <https://orcid.org/0000-0001-5945-4435>

Novel *STAT3* Y360C Gain-of-function Variant Underlies Immune Dysregulation and Aberrancy in Mitochondrial Dynamics

Kornvalee Meesilpavikkai ^{1,2,3,*}, Kasiphak Kaikaew ⁴, Zijun Zhou ^{1,2,5}, Virgil A.S.H. Dalm ^{1,2,5}, Fabian M.P. Kaiser ^{1,6}, Christopher Schliehe ⁷, Sigrid M.A. Swagemakers ⁸, Peter J. van der Spek ⁸, Benjamin Schrijver ^{1,5}, Pamela Vasic¹, Maaïke de Bie¹, Marleen Bakker ⁹, Chiara Milanese ¹⁰, Pier G. Mastroberardino ¹⁰, Nattiya Hirankarn ^{11,*}, Narissara Suratannon ¹², Hanna IJspeert ¹, Willem A. Dik ¹, P. Martin van Hagen^{1,2,5}

¹Laboratory Medical Immunology, Department of Immunology, Erasmus University Medical Center, 3015 GD Rotterdam, The Netherlands

²Division of Clinical Immunology, Department of Internal Medicine, Erasmus University Medical Center, 3015 GD Rotterdam, The Netherlands

³Department of Microbiology, Faculty of Medicine, Chulalongkorn University, Bangkok10330, Thailand

⁴Center of Excellence in Alternative and Complementary Medicine for Gastrointestinal and Liver Diseases, Department of Physiology, Faculty of Medicine, Chulalongkorn University, Bangkok10330, Thailand

⁵Academic Center for Rare Immune Diseases (RIDC), Erasmus University Medical Center, 3015 GD Rotterdam, The Netherlands

⁶Department of Neonatal and Pediatric Intensive Care, Erasmus University Medical Center - Sophia Children's Hospital, 3015 GD Rotterdam, The Netherlands

⁷Department of Immunology, Erasmus University Medical Center, 3015 GD Rotterdam, The Netherlands

⁸Department of Pathology and Bioinformatics, Erasmus University Medical Center, 3015 GD Rotterdam, The Netherlands

⁹Department of Pulmonary Medicine, Erasmus Medical Center, 3015 GD Rotterdam, The Netherlands












¹⁰Department of Molecular Genetics, Erasmus University Medical Center, 3015 GD Rotterdam, The Netherlands

¹¹Center of Excellence in Immunology and Immune-mediated Diseases, Department of Microbiology, Faculty of Medicine, Chulalongkorn University, Bangkok10330, Thailand

¹²Division of Allergy and Immunology, Department of Pediatrics, Faculty of Medicine, Chulalongkorn University, Bangkok10330, Thailand

ABSTRACT

The *STAT3* is an important regulator in a wide range of different cell types. Human *STAT3* variants are associated with several immune dysregulation diseases. The current study investigated the clinical, genetic, and immunobiological data obtained from a family with novel heterozygous *STAT3* variants located at p.Y360C of the DNA binding domain. The clinical manifestations of these patients include autoimmunity, immunodeficiency, and postnatal growth defects. Broad *STAT3* regulated cells including patient primary immune cells and HEK293 cells harboring the variant were assessed. Remarkably high levels of *STAT3*-regulated cytokines were detected in the sera of the patients. *STAT3* nuclear binding and *STAT3* activity were higher in *STAT3*-transduced HEK293 cells containing the p.Y360C variant when compared to HEK cells expressing wild type (WT) *STAT3*. Upon cytokine activation, *STAT3* variants inhibited nuclear translocation of the WT *STAT3* molecule. We also demonstrated that PBMCs from these patients exhibit significantly higher mitochondrial activity compared to that of healthy controls. The exploration of the effects of *STAT3* Y360C

Fabian M.P. Kaiser 
<https://orcid.org/0000-0002-0335-2859>
 Christopher Schliehe 
<https://orcid.org/0000-0002-1923-8620>
 Sigrid M.A. Swagemakers 
<https://orcid.org/0000-0003-4339-8189>
 Peter J. van der Spek 
<https://orcid.org/0000-0002-2203-0652>
 Benjamin Schrijver 
<https://orcid.org/0000-0002-6427-6765>
 Marleen Bakker 
<https://orcid.org/0000-0001-6965-5767>
 Chiara Milanese 
<https://orcid.org/0000-0001-8696-2603>
 Pier G. Mastroberardino 
<https://orcid.org/0000-0003-2364-4258>
 Nattiya Hirankarn 
<https://orcid.org/0000-0003-2224-6856>
 Narissara Suratannon 
<https://orcid.org/0000-0003-1182-3611>
 Hanna IJspeert 
<https://orcid.org/0000-0002-7061-5321>
 Willem A. Dik 
<https://orcid.org/0000-0001-5235-3156>

Conflict of Interest

The authors declare no potential conflicts of interest.

Abbreviations

AD-HIES, autosomal dominant hyper-IgE syndrome; ECAR, extracellular acidification rate; EMSA, electrophoretic mobility shift assay; FCCP, carbonyl cyanide-p-trifluoromethoxyphenylhydrazone; FCS, fetal calf serum; GH, growth hormone; GOF, gain-of-function; IVIG, intravenous immunoglobulin; LBT, liver biochemistry tests; LOF, loss-of-function; OCR, oxygen consumption rate; pSTAT, phosphorylated STAT; SOCS3, suppressor of cytokine signaling 3; WT, wild type.

Author Contributions

Conceptualization: Meesilpavikkai K, Dalm VA; Data curation: Meesilpavikkai K, Zhou Z, Dalm VA, Kaiser FM, Schliehe C; Formal analysis: Meesilpavikkai K, Kaikaew K, Kaiser FM, Swagemakers SM, Schrijver B; Funding acquisition: Meesilpavikkai K; Investigation: Meesilpavikkai K, Schrijver B, Vasic P, de Bie M, Milanese C, Mastroberardino PG; Methodology: Meesilpavikkai K; Project administration: Martin Van Hagen P, Hirankarn N; Resources: Meesilpavikkai K, Martin Van Hagen P, Hirankarn N; Supervision: Dalm VA, Dik WA, Martin Van Hagen P, Hirankarn N; Validation: Kaikaew K, Schliehe C, Swagemakers SM; Writing - original draft:

variants described in our study provides novel insights into the molecular effects of the STAT3 variant and its role in the pathophysiology of *STAT3* gain-of-function syndromes.

Keywords: Immune system disorder; Gain of function mutation; Electrophoretic mobility shift assay; Cell respiration; Nuclear transport

INTRODUCTION

The STAT family comprises 7 members of transcription factors that mediate diverse cellular responses to cytokines, growth factors, and hormones (1). These proteins are crucial for relaying signals from the cell membrane receptors to the nucleus, where they regulate gene expression. In mammals, the STAT family includes STAT1, STAT2, STAT3, STAT4, STAT5A, STAT5B, and STAT6. Among these, the STAT3 signaling pathway has gained considerable attention for its involvement in a plethora of physiological processes, including cell survival, proliferation, differentiation, angiogenesis, and immune regulation, as well as its significant role in various pathological conditions, particularly cancer, autoimmune diseases, and immunodeficiencies (2-5).

Several cytokines and hormones activate STAT3 through interactions with cell surface receptors, including the receptors for IL-6, IL-10, IL-21, IL-23, IFNs, growth hormone (GH), and epidermal growth factor (6-8). IL-6, in particular, is recognized as a classic immune activator of STAT3 (9). Binding of IL-6 to the IL-6 receptor results in the formation of an IL-6/IL-6R/gp130 complex, which subsequently activates JAK1 and JAK2. These kinases then phosphorylate STAT3 at tyrosine residue 705 (10,11). The phosphorylated STAT3 (pSTAT3) molecules form dimers and translocate to the nucleus, where they initiate the transcription of target genes (12). In addition to forming homodimers, pSTAT3 can heterodimerize with other STAT family members, such as STAT1, STAT5A, and STAT5B, depending on the activating stimulus (13). Interestingly, some studies suggest that phosphorylation is not always required for STAT3 nuclear translocation, as unphosphorylated monomeric or dimeric STAT3 can also accumulate in the nucleus (14-17).

STAT3-mediated signaling is crucial for the differentiation of T-helper (Th) 17 lymphocytes (2,18). Th17 polarization of naïve T cells increased in adult mice with a *STAT3* gain-of-function (GOF) variant (19). STAT3 signaling is tightly controlled by several mechanisms including the upregulation of a suppressor of cytokine signaling 3 (*SOCS3*), which is a downstream target gene of STAT3 (20,21). The *SOCS3* protein is a well-known JAK/STAT3 pathway feedback inhibitor. It achieves this by binding to gp130 or obstructing the activity of JAK2, thereby creating a negative feedback loop that limits STAT3 activation. However, *SOCS3* does not regulate all cytokine receptors that activate STAT3 and prolonged STAT3 activation by IL-6 might not be controlled by *SOCS3* (20,21). In addition to its role in STAT3 regulation, *SOCS3* modulates the signaling of other STAT proteins and pathways unrelated to STAT thus affecting infection and inflammatory responses (20,22,23).

Besides its classical function as nuclear transcription factor, STAT3 also localizes in mitochondria (mitoSTAT3) where it displays alternative functions known as non-classical STAT3 functions (24). MitoSTAT3 is a positive regulator of complexes I, II, and V of the electron transport chain (24-26). In addition to regulating cellular metabolism, mitoSTAT3 participates in various cellular events including cell development, cell death, inflammation,

Meesilpavikkai K; Writing - review & editing: Kaikaew K, Zhou Z, Dalm VA, Kaiser FM, Schliehe C, Swagemakers SM, Van Der Spek PJ, Bakker M, Mastroberardino PG, Suratannon N, Ijspeert H, Dik WA, Martin Van Hagen P, Hirankarn N.

and T lymphocyte immunity (24). Upon activation of CD4⁺ T lymphocytes by IL-6, STAT3 accumulates in the mitochondria, elevates mitochondrial membrane potential (MMP), and promotes the formation of mitochondrial respiratory supercomplexes (27,28). mitoSTAT3 also binds mitochondrial DNA and is related to the transcriptional regulation of the mitochondrial genome (29).

STAT3 variants are associated with severe immune dysregulation. Dominant-negative loss-of-function (LOF) variants of *STAT3* are linked to autosomal dominant hyper-IgE syndrome (AD-HIES or Job's syndrome), where patients exhibit impaired IL-6 responses and a marked reduction in IL-17-producing Th17 lymphocytes (6,30-32). Clinically, AD-HIES is characterized by increased susceptibility to bacterial infections, particularly in the lungs and skin, along with eczema and elevated serum IgE levels (30-37). Conversely, patients with *STAT3* GOF variants suffer from prominent early-onset multi-organ immune dysregulations (38,39). Clinical manifestations of patients with *STAT3* GOF syndrome are diverse, but commonly include autoimmune cytopenias, lymphoproliferation, skin disorders, enteropathy, interstitial lung disease, growth defects, immunodeficiency, and endocrinopathies (6,38-40). Increased intrinsic *STAT3* transcriptional activity or elevated expression of *STAT3*-target genes, including *SOCS3*, are mostly detected in cells carrying the *STAT3* GOF variant (41-44). Interestingly, *STAT3* hyperphosphorylation is typically absent in these cases. Instead, some studies report reduced phosphorylation of *STAT1* and/or *STAT5*, potentially contributing to immunodeficiency and growth defects, respectively (41,44-46).

In this study, we describe a novel germ-line heterozygous *STAT3* Y360C variant. We evaluated the immunobiological phenotypes from broad *STAT3* regulated cells including primary immune cells derived from the patients and HEK293 cells harboring the variant. Our findings substantiated the importance of *STAT3* as a crucial regulator of immune function. Additionally, we provide immunometabolic characteristics of this *STAT3* variant. Although comprehensive clinical overviews of *STAT3* GOF variants have been reported, further immunophenotyping and biological characterization data remain necessary to elucidate the diverse clinical phenotypes observed in patients with *STAT3* GOF syndrome. This study aimed to significantly enhance our understanding of the variable clinical spectrum associated with *STAT3* GOF variants, thereby contributing to a broader knowledge of immune regulation and its implications.

MATERIALS AND METHODS

Patient consent and regulatory compliance

Informed consent was obtained from all enrolled participants. The study protocol including blood sampling from healthy controls was approved by the Institutional Review Board of the Erasmus MC, University Medical Center, Rotterdam, with ethics approval numbers MEC 2013-026 and MEC-2016-202. The study protocol was in accordance with the principles of the Declaration of Helsinki.

Long-term T lymphocyte culture

Long-term cultures of T lymphocytes from both patients and healthy controls were isolated from PBMCs via an EasySep™ Human T Cell Isolation Kit (STEMCELL Technologies, Köln, Germany). The cells were cultured and expanded in RPMI-1640 medium containing 10% heat inactivated human serum (Sigma-Aldrich, Saint Louis, MO, USA), 2% penicillin and

streptomycin (Cambrex BioWhittaker, Verviers, Belgium), 1 µg/ml phytohemagglutinin (Sigma-Aldrich), 25 IU/ml IL-2 (Novartis, Basel, Switzerland) and 12.5 ng/ml IL-15 (BioLegend, San Diego, CA, USA), in the presence of γ -irradiated (40 Gy) allogeneic PBMCs, Hal01 and RS411 B cell lines. After 2 wk of expansion, cultured cells were checked for expression of the T lymphocyte surface marker, CD3 (BD Biosciences, San Jose, CA, USA) by flow cytometry, confirming that all long-term T lymphocyte cultures contained >95% CD3+ expressing cells.

Plasmids and site-specific mutagenesis

The pLEGFP-WT-STAT3 plasmid (Addgene, Watertown, MA, USA) was mutated into c.1079A>G via site-specific mutagenesis (QuikChange Site-Directed Mutagenesis Kit; Agilent Technologies, Santa Clara, CA, USA) according to the manufacturer's protocol. Following confirmation by Sanger sequencing, STAT3 construct was extracted from the pLEGFP plasmid and cloned into a Gateway-compatible pCW57.1 plasmid (Addgene #41393) using the pENTR™ Directional TOPO® cloning Kit and the Gateway® LR Clonase™ II Enzyme Mix (Invitrogen, Thermo Fisher Scientific, Waltham, MA, USA). The final expression constructs were confirmed by Sanger sequencing.

HEK293 cell culture and transduction

Lentiviral production of the pCW57.1 plasmid construct was carried out in HEK293FT packaging cells (kindly provided by Bram van der Eerden) using a ViraPower plasmid (kindly provided by Jenny A. Visser) and Eugene 6 (Promega Corporation, Madison, WI, USA). Two days after transfection, media containing lentiviral particles were harvested and transferred to HEK293 cells (kindly provided by Jenny A. Visser). Cells were cultured with lentiviral particles overnight, after which the media were replaced with fresh growth media. The cells were then grown and expanded under puromycin selection for 2 wk. Single cell dilution was performed to obtain clonal populations. Total STAT3 levels expressed by the clones were measured by intracellular flow cytometry using FITC-conjugated anti-STAT3 (BD Biosciences). Three clones of both the STAT3 variant and STAT3 wild type (WT), displaying similar total STAT3 levels, were selected for further expansion and subsequent experiments.

Flow cytometry

Th subset analysis was performed on isolated PBMCs of patients and healthy controls. Cells were stained with fluorochrome-conjugated human-specific antibodies (BD Biosciences) in PBS containing 1% fetal calf serum (FCS) and 0.09% sodium azide for 30 min and analyzed on a BD LSRFortessa™ cell analyzer. Th cells (CD4+CD45RA-) were further subdivided into Th1 (CCR6-CXCR3+), Th2 (CCR6-CXCR3-), Th17 (CCR6+CXCR3-CCR10-), Th22 (CCR6+CXCR3-CCR10+), and Treg (CD25+CD127^{low}).

For STAT phosphorylation experiments, long-term T lymphocyte cultures were starved in serum-free medium for 1 h and thereafter stimulated with IL-6 (100 ng/ml; R&D systems, Minneapolis, MN, USA), IFN- α (10⁴ IU/ml; PeproTech, London, UK), IL-21 (200 ng/ml; Thermo Fisher Scientific), or IL-2 (100 IU/ml; Novartis). After stimulation, cells were fixed and permeabilized with reagents according to the manufacturer's protocol (Phospho-Epitopes Exposure kit; Beckman Coulter, Brea, CA, USA). Subsequently, all samples were stained with fluorochrome-conjugated anti-total STAT3 (M59-50; BD Biosciences), anti-pSTAT1 (58D6; Cell Signaling Technology, Danvers, MA, USA), anti-pSTAT3 (D3A7; Cell Signaling Technology), or anti-pSTAT5 (C71E5; Cell Signaling Technology), with dilution according to the manufacturer's protocol, for 30 min and measured with a BD FACSCanto™ II machine.

Immunofluorescence

HEK293 cells were transfected with pCW57.1 STAT3 WT or the same plasmid containing STAT3 Y360C variant using Lipofectamine 3000 transfection reagent (Thermo Fisher Scientific). After 24 h of transfection, cells were detached and cultured on coverslips placed in 6-well culture plates. Cells were incubated for an additional 24 h to ensure firm attachment and were subsequently starved in serum-free medium for 1 h before stimulation. Following 30 min of stimulation with IFN- α (10^4 IU/ml; PeproTech), cells were immediately fixed with 4% paraformaldehyde for 15 min at room temperature and permeabilized with 100% methanol for 10 min at -20°C . The cells were stained overnight with STAT3 Mouse mAb (1:1,600 [124H6; Cell Signaling Technology]) and Phospho-Stat3 (Tyr705) XP[®] Rabbit mAb (1:1,000 [D3A7; Cell Signaling Technology]). Cells were then incubated for 2 h with secondary antibodies: donkey-anti-rabbit-TRITC (1:500 dilution; Thermo Fisher Scientific) and F(ab')₂-Goat anti-Mouse IgG (H+L) Cross-Adsorbed Secondary Antibody, Alexa Fluor 488 (1:1,000 dilution; Thermo Fisher Scientific). The coverslips were mounted using VECTASHIELD Antifade Mounting Medium with DAPI (Vector Laboratories, Burlingame, CA, USA) and sealed with nail polish. Images were obtained using Zeiss AxioVert 100 using a 20 \times objective lens.

To compare the nuclear translocation between STAT3 WT and the Y360C variant, HEK293 cells were transfected with pCW57.1 STAT3 WT or the same plasmid containing STAT3 Y360C variant (both FLAG-tagged) and the plasmid pEGFP-N1-STAT3 WT (Addgene #111934), using Lipofectamine 3000 transfection reagent (Thermo Fisher Scientific). After 24 h of transfection, cells were detached and cultured on coverslips placed in 6-well culture plates. Cells were then incubated, stimulated, fixed, and permeabilized as described above. For immunofluorescence staining, cells were blocked with 5% human serum in combination with 0.3% Triton[™] X-100 in PBS for 1 h and stained with rabbit-anti-human pSTAT3 (1:1,000 [D3A7; Cell Signaling Technology]) and mouse anti-FLAG (1:1,000 [9A3; Cell Signaling Technology]) overnight. Cells were thereafter incubated for 2 h with secondary antibodies, donkey-anti-rabbit-TRITC (1:500 dilution, Thermo Fisher Scientific) and goat-anti-mouse-Alexa Fluor 647 (1:500 dilution, Thermo Fisher Scientific). The coverslips were mounted using VECTASHIELD Antifade Mounting Medium with DAPI (Vector Laboratories) and sealed with nail polish. Confocal fluorescence images were obtained using a Leica confocal system (Leica TCS SP5 II; Leica Microsystems CMS GmbH, Wetzlar, Germany), equipped with diode laser (405 nm), Argon laser (488 nm), DPSS laser (561 nm) and a helium-neon laser (633 nm). Images were taken using a 63 \times /1.4 oil objective and recorded with standard LAS-AF software (version 2.6.3; Leica Microsystems CMS GmbH). Possible spectral overlap between different fluorochromes was avoided by careful compensation of imaging conditions and sequential scanning. Fluorescent intensity and nucleocytoplasmic localization were quantified using ImageJ (National Institutes of Health, Bethesda, MD, USA).

ELISA

Serum concentrations of IL-6, IL-17A, and IL-17F from both patients and healthy controls were measured using ELISA kits (IL-6 Human Matched Antibody Pair; Thermo Fisher Scientific, Human IL-17A and F DuoSet ELISA; R&D systems). To determine IL-6 production by PBMCs, the cells were first incubated in RPMI medium without FCS, then stimulated with 81 nM phorbol 12-myristate 13-acetate and 1.3 μM ionomycin (Cell Stimulation Cocktail (500 \times); Thermo Fisher Scientific). After 48 h of stimulation, the supernatants were collected for IL-6 measurement by ELISA.

Electrophoretic mobility shift assay (EMSA)

Lentiviral transduced HEK293 cells were stimulated with IFN- α (10^4 IU/ml; PeproTech) for 30 min. After stimulation, cells were collected for nuclear extraction with NE-PER™ Nuclear and Cytoplasmic Extraction Reagents (Thermo Fisher Scientific) according to the manufacturer's protocol. Nuclear lysates were incubated for 10 min with binding buffer containing 3% Ficoll, 1 mM DTT, 5 mM MgCl₂, 0.05 μ g/ μ l poly (dI-dC), and UltraPure™ Salmon Sperm DNA Solution (Thermo Fisher Scientific). The reaction mixtures were incubated for an additional 20 min with STAT3 oligo hSIE (high-affinity sis-inducible element, m67 variant, 5'-AGCTTCATTTCCCGTAAATCCCTA) in the dark. The protein-DNA complexes were fractionated in 5% non-denaturing TBE-polyacrylamide gels and detected with an Odyssey IR imaging system (LI-COR Biotechnology, Bad Homburg, Germany). The images were quantified using Image Studio Lite software (version 5.2; LI-COR Biotechnology).

Reverse transcription quantitative real-time PCR

STAT3-transduced HEK293 cells were starved in serum-free medium for 1 h and subsequently stimulated with IL-6 10 ng/ml (R&D systems) or IFN- α 10^3 IU/ml (PeproTech). After stimulation, the cultured cells were harvested, and RNA was extracted using the GenElute Mammalian Total RNA Miniprep Kit (Sigma-Aldrich). cDNA was synthesized from the RNA using random primers (Thermo Fisher Scientific). PCR for *SOCS3* was achieved with TaqMan Universal PCR Master Mix (Thermo Fisher Scientific) and predesigned TaqMan® MGB probes (Thermo Fisher Scientific): glyceraldehyde-3-phosphate dehydrogenase (*GAPDH*; Hs99999905_m1) and *SOCS3* (Hs02330328_s1). Thermocycling was performed on the QuantStudio 5 Flex Real-Time PCR machine (Thermo Fisher Scientific). The expression level of *SOCS3* was analyzed using the $2^{-\Delta\Delta CT}$ method, normalized to the housekeeping gene, *GAPDH*.

Luciferase reporter assay

STAT3-transduced monoclonal HEK293 cells were co-transfected with pRL-SV40 and pGL4.47[luc2P/SIE/Hygro] vector plasmid (Promega Corporation). After 48 h of transfection, the cells were starved for 1 h and stimulated with IL-6 (10 ng/ml; R&D systems) or IFN- α (10^3 IU/ml; PeproTech). Following the stimulation, Firefly and Renilla luminescence was measured using the Dual-Glo® Luciferase Assay System (Promega Corporation). STAT3 activity was determined by calculating the ratio of Firefly to Renilla luminescence.

Metabolic assay

Bioenergetic profiles of PBMCs were generated using a Seahorse XF24 Extracellular Flux Analyzer (Seahorse Bioscience, Billerica, MA, USA). Oxygen consumption rates (OCRs) and glycolysis (extracellular acidification rate [ECAR]) of the cells were measured simultaneously in real-time (47). A Seahorse XF-24 plate was coated with Cell-Tak (22.4 μ g/ml; BD Biosciences) to enable cell adhesion. Patient and healthy control PBMCs were seeded on the plate at a density of 8×10^5 cells/well. The plate was incubated at 37°C for 30 min in the presence of CO₂ in unbuffered DMEM (XF Assay Medium; Agilent Technologies) in which pH was set at 7.4 on the day of the experiment and supplemented with 5 mM of glucose and 1 mM of pyruvate. Subsequently, the plate was incubated at 37°C without CO₂ for 30 min before being moved to the Seahorse machine for analysis. After OCR and ECAR were measured at the baseline level, sequential injections of 0.5 μ M oligomycin (ATP synthase inhibitor), 0.5 μ M carbonyl cyanide-p-trifluoromethoxyphenylhydrazone (FCCP, mitochondrial respiration uncoupler), 0.5 μ M rotenone (complex I inhibitor), and 0.5 μ M antimycin (complex III inhibitor) were administered.

RESULTS

Clinical phenotypes of patients with identified STAT3 variant

A family with 2 clinically affected individuals was enrolled in this study (Fig. 1A). The clinical disease spectrum of the patients was heterogeneous and overlapped with that of previously published cases of STAT3 GOF variants. Proband II-2 was a female patient with a height of 157 cm (−2.1 SD) and disproportionately short arms and legs. Endocrine investigation of her short stature revealed a low serum IGF-1 level (4.1 nmol/l; normal range 13–35 nmol/l), a low serum insulin-like growth factor-binding protein 3 level (1.7 µg/l; normal range 3.3–6.6 µg/l), while her basal GH (1.2 µg/l) and peak GH concentrations, following a GH releasing hormone-arginine stimulation test (51.1 µg/l), was normal, suggesting GH insensitivity.

The patient was splenectomised when she was 25 years of age due to recurrent autoimmune thrombocytopenic purpura and splenomegaly. Her medical history revealed recurrent

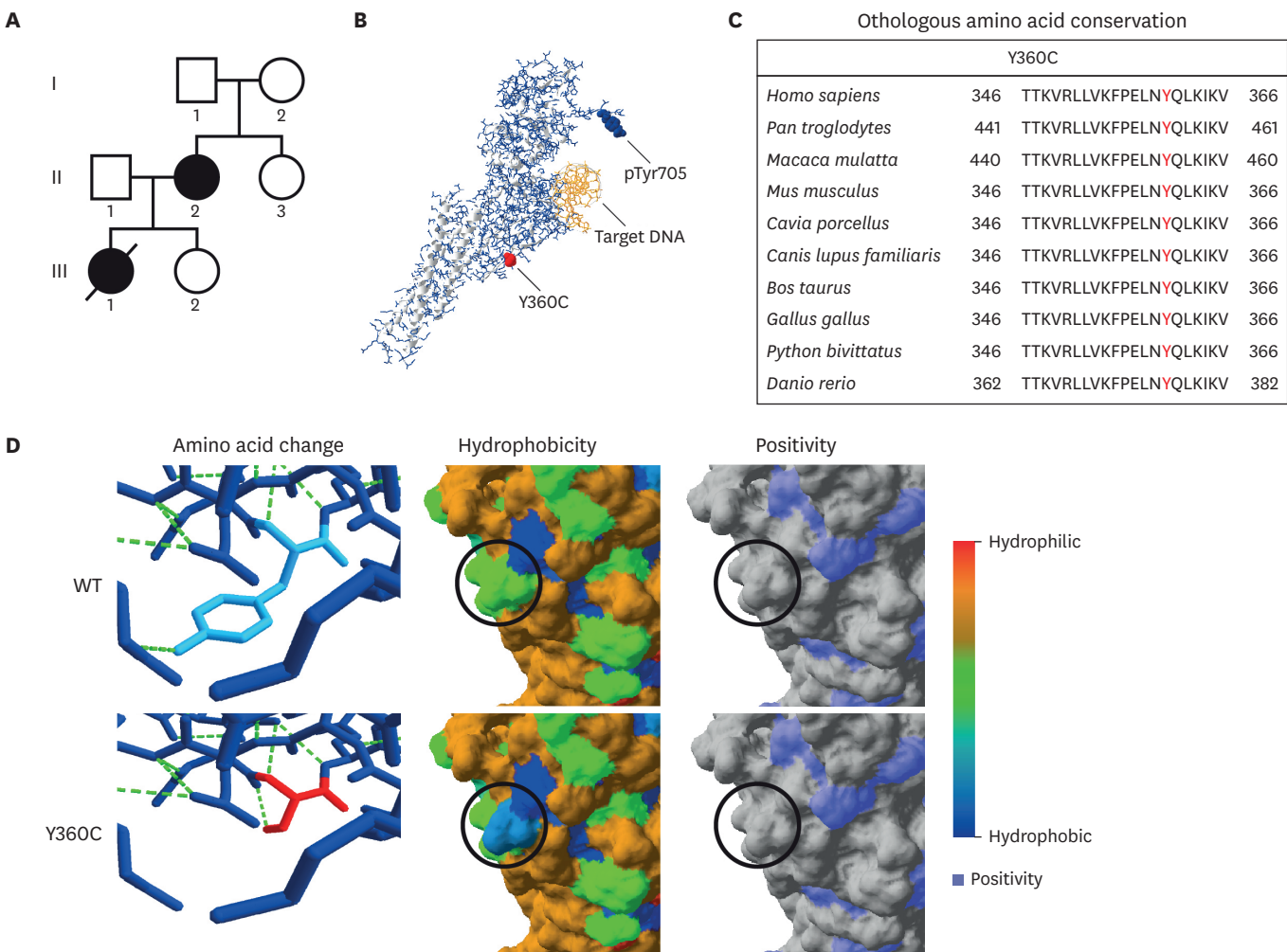


Figure 1. Novel heterozygous STAT3 variants. (A) A family pedigree of patients with STAT3 Y360C variant. Dark symbols indicate clinically affected individuals. Deceased patients are depicted as a diagonal line through symbols. (B) Three-dimensional structure of pSTAT3 bound to target DNA. The Y360C variant is indicated as well as the tyrosine 705 phosphorylation site. (C) Evolutionary conservation of p.Tyr360 among indicated species. (D) Predicted effects of STAT3 Y360C variant as obtained from Protein Data Bank models. Amino acid replacement from WT (blue) into Y360C variant (red) is shown in the left column. The green dashed lines indicate hydrogen bonds. Predicted changes of the STAT3 molecular surface are colored according to hydrophobicity (middle column) and positivity (right column). Circles indicate the location of the Y360C variant.

bacterial respiratory tract infections, persistent chronic EBV infection, and other viral infections including influenza, rhinovirus, adenovirus infections, and herpes zoster reactivation. Other isolated organisms included *Staphylococcus aureus*, *Pseudomonas aeruginosa*, *Stenotrophomonas maltophilia*, and *Haemophilus influenzae*. IgA, IgG2, and IgG4 deficiency were diagnosed at the age of 30, followed by intravenous immunoglobulin (IVIG) substitution therapy. She developed bronchiectasis following several episodes of pulmonary infections. Her additional medical history includes dermatitis, hemangioma, lymphadenopathy, and abnormal liver biochemistry tests (LBT). Currently, she was diagnosed with end-stage lung disease with severe pulmonary hypertension and congestive heart disease. Although treated with anti-IL-6 therapy (tocilizumab) she did not show significant clinical improvement. During tocilizumab therapy, she developed a psoriasis-like lesion on the big toe superimposed by local staphylococcal and herpes zoster infections. Initiation of the JAK inhibitor (tofacitinib) resulted in significant relief of clinical signs including pulmonary hypertension, but the treatment was paused due to local cryptococcal infection of the toe. After prolonged fluconazole therapy, the lesion subsided with a negative microbial culture. Reintroduction of tofacitinib (5 mg/daily) was initiated afterward and the therapy improved her well-being significantly. Now not only pulmonary hypertension but also congestive heart disease is completely under control during tofacitinib treatment. However, the contribution of tofacitinib to this remission is speculative. In late 2024, she experienced a 2-month history of fever and generalized lymphadenopathy. She had recurrent infections, including rhinoviral, adenoviral, oral herpes simplex, and fungal infections. Additionally, increased cytomegalovirus and Epstein-Barr virus viral loads were detected. She was treated with valganciclovir, which resulted in a reduction of fever. However, a high-positive Toxoplasma PCR was also detected in peripheral blood. Consequently, the patient was treated with pyrimethamine and sulfadiazine, leading to an improvement in her clinical condition.

Proband III-1, a daughter of proband II-2, was of normal height with the general appearance of frontal bossing. She experienced autoimmune thrombocytopenia and leucopenia at the age of 10. She had poor pneumococcal vaccination response, recurrent otitis media, recurrent pulmonary infection, and herpes zoster reactivation. Causative agents included *Pseudomonas* spp., *S. aureus*, *Acinetobacter* spp., herpes simplex virus, influenza B virus, coronavirus, and adenovirus. IgA and IgG2 deficiency were found at the age of 16 and IVIG therapy was initiated. Hepatosplenomegaly with abnormal LBT and lymphadenopathy was also noted in her medical history. She experienced eczematous rashes on all of her extremities and the skin biopsy examination revealed non-infectious granulomatous inflammation. She was treated with anti-B-cell therapy (rituximab) which initially led to improvement of her dyspnea and a reduction in spleen size. Following multiple episodes of pulmonary infections, the patient developed bronchiectasis. She subsequently succumbed to refractory pulmonary hypertension at the age of 25. Despite treatment with diuretics, bosentan, sildenafil, prostacyclins, and immune-modulating agents such as tocilizumab and tofacitinib, her condition remained unresponsive.

Both of the index patients carried a novel heterozygous variant in exon 11 of *STAT3* at c.1079A>G. This variant resulted in the replacement of tyrosine by cysteine at position 360 (STAT3:c.1079A>G; p.Tyr360Cys; NM_139276.3) and was predicted as “tolerated” by the Sort Intolerant From Tolerant algorithm (score: 0.14), “possibly damaging” by the Polymorphism Phenotyping v2 (PolyPhen-2 score: 0.999), CADD score 29.2 (CADD GRCh38-v1.7), and “disease-causing” by Mutation Taster. This identified variant has not been reported as single nucleotide polymorphisms in the National Center of Biotechnology Information, GnomAD, and other control cohorts.

The amino acid replacement of p.[Y360C] is located at evolutionary highly conserved positions in the DNA binding domain of STAT3 and exposed on the outer surface of the molecule (**Fig. 1B-C**). Although this amino acid replacement was not predicted to significantly affect the overall structure of the STAT3 molecule, the local surface region appeared more hydrophobic without a charge alteration (**Fig. 1D**).

Elevated serum levels of STAT3-regulated cytokines and Th17 lymphocytes in the blood of patients

Blood samples from enrolled patients and gender-ethnicity-matched healthy controls were collected for immunological evaluation. Serum levels of the STAT3-regulated cytokines, IL-6, IL-17A, and IL-17F, were markedly elevated in the patients when compared to healthy controls, in whom these cytokines were nearly undetectable (**Fig. 2A**). By contrast, IL-6 production in the PBMCs of patients was reduced following PMA/ionomycin stimulation, in comparison to PBMCs from healthy controls (**Fig. 2B**). The finding of high circulating IL-6 in combination with diminished capacity of PBMCs to produce IL-6 upon activation is substantiated by previous findings, and may be explained by a compensatory mechanism caused by

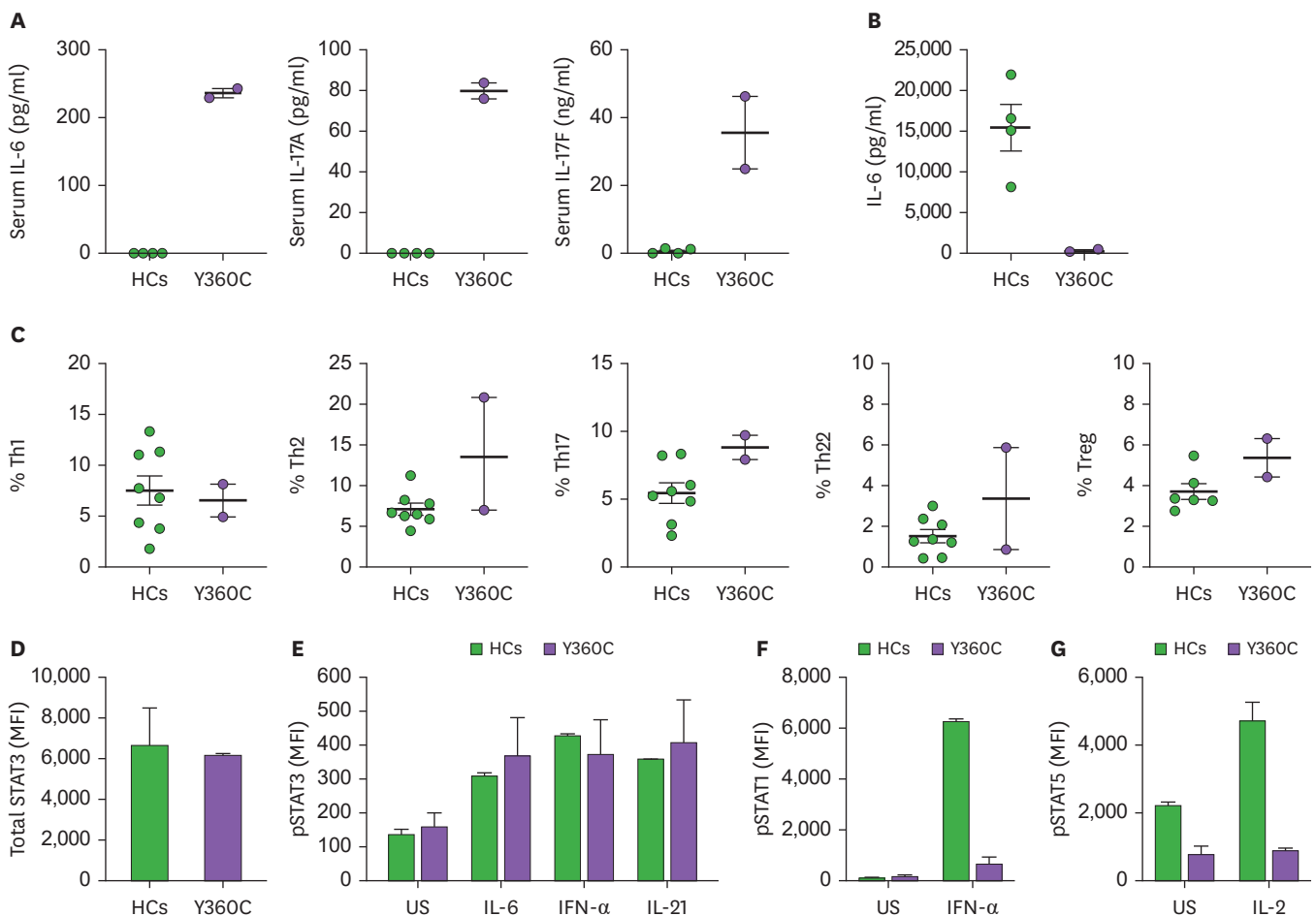


Figure 2. Immunological characteristics of patients with STAT3 Y360C variant. (A) Serum levels of IL-6, IL-17A, and IL-17F. (B) IL-6 production by PBMCs stimulated with PMA/ionomycin. (C) Percentages of Th1, Th2, Th17, and Treg subsets in peripheral blood. (D-G) Assessment of STAT phosphorylation in long-term T lymphocyte cultures of patients and HCs: MFI of total STAT3 (D); MFI of pSTAT3 (E); MFI of pSTAT1 (F); and MFI of pSTAT5 (G). Data are expressed as mean \pm SEM. Data representative of 3 independent experiments. HC, healthy control; MFI, mean fluorescence intensity; US, unstimulated.

excessive IL-6 overexposure *in vivo* (48). Considering that STAT3 signaling is essential for the generation of Th17 lymphocytes, we assessed Th-subsets and regulatory T lymphocytes (Treg) in freshly isolated PBMCs. The frequency of Th17 lymphocytes was slightly higher in patients with Y360C *STAT3* variants in comparison to the controls. However, this difference is not substantial (**Fig. 2C**). Frequencies of Th1, Th2, and Th22 did not differ between patients and healthy controls. Previous reports have indicated decreased Treg numbers in several cases of *STAT3* GOF (39,41,43). In our study, however, we observed a marginal increase in Treg percentage in patients carrying the *STAT3* Y360C variant (**Fig. 2C**).

STAT3 phosphorylation in T lymphocytes is not affected by *STAT3* variants

To examine the effect of variants on *STAT3* phosphorylation, long-term T lymphocyte cultures were established from patient-derived PBMCs. Long-term T lymphocyte cultures were used for this purpose in order to reduce the potential confounding effects of *in vivo* pathogens and/or therapy to which patient PBMCs may have been exposed (49). Total *STAT3* levels in T lymphocytes did not differ between patients and healthy controls (**Fig. 2D**). Moreover, *STAT3* phosphorylation levels following stimulation with IL-6, IFN- α , or IL-21 were comparable between patient and healthy control cells (**Fig. 2E**). Given that some clinical features of patients with *STAT3* GOF variants were also observed in patients with *STAT1* and *STAT5b* LOF variants (40,41,46), phosphorylation of these *STAT* molecules was investigated. *STAT1* phosphorylation was clearly diminished in the T lymphocytes of the patients carrying the *STAT3* Y360C variant following IFN- α stimulation (**Fig. 2F**). Additionally, a decrease in *STAT5* phosphorylation following IL-2 stimulation was also observed in these patients, which might correlate with the growth delay (**Fig. 2G**).

STAT3 Y360C ablates nuclear migration of WT *STAT3*

HEK293 cells express low endogenous levels of *STAT3*. To investigate the impact of *STAT3* Y360C variants on nuclear translocation, HEK293 cells were transfected with plasmids encoding either *STAT3* WT or *STAT3* Y360C. In the absence of stimulation, *STAT3* was clearly localized in the cytoplasm. Upon treatment with IFN- α for 30 min, p*STAT3* was detected in the nucleus. Cells carrying the *STAT3* Y360C variant exhibited stronger nuclear fluorescence intensity of p*STAT3* compared to those expressing *STAT3* WT (**Supplementary Fig. 1**).

HEK293 cells were also transfected with a plasmid encoding either GFP-tagged *STAT3* WT, FLAG-tagged *STAT3* WT, or FLAG-tagged *STAT3* Y360C. In the absence of stimulation, all *STAT3* were clearly localized in the cytoplasm (**Fig. 3A-E**, upper rows). Upon treatment with IFN- α , the localization of *STAT3* and p*STAT3* was assessed. GFP-tagged and FLAG-tagged *STAT3* WT, *STAT3* Y360C, and p*STAT3* were prominently observed in the nucleus and were detected at negligible levels in the cytoplasm, indicating complete nuclear translocation of *STAT3* (**Fig. 3A-C**, lower rows).

Since these patients carry a heterozygous *STAT3* Y360C variant, we next examined the effect of *STAT3* Y360C on *STAT3* WT protein by co-transfecting HEK293 cells with a plasmid expressing GFP-tagged *STAT3* WT and a plasmid expressing a FLAG-tagged *STAT3* Y360C variant. Co-transfection of GFP-tagged *STAT3* WT and FLAG-tagged *STAT3* WT was used as a control. In these control cells, both GFP and FLAG-labelled *STAT3* as well as p*STAT3* were detectable in the nucleus after IFN- α stimulation (**Fig. 3D**, lower row). Upon IFN- α stimulation, FLAG-tagged *STAT3* Y360C migrated to the nucleus (**Fig. 3E**, lower row) comparable to that observed in the homozygous situation (**Fig. 3A-C**, lower rows). However, some GFP-tagged *STAT3* WT remained in the cytoplasm after stimulation while FLAG-tagged

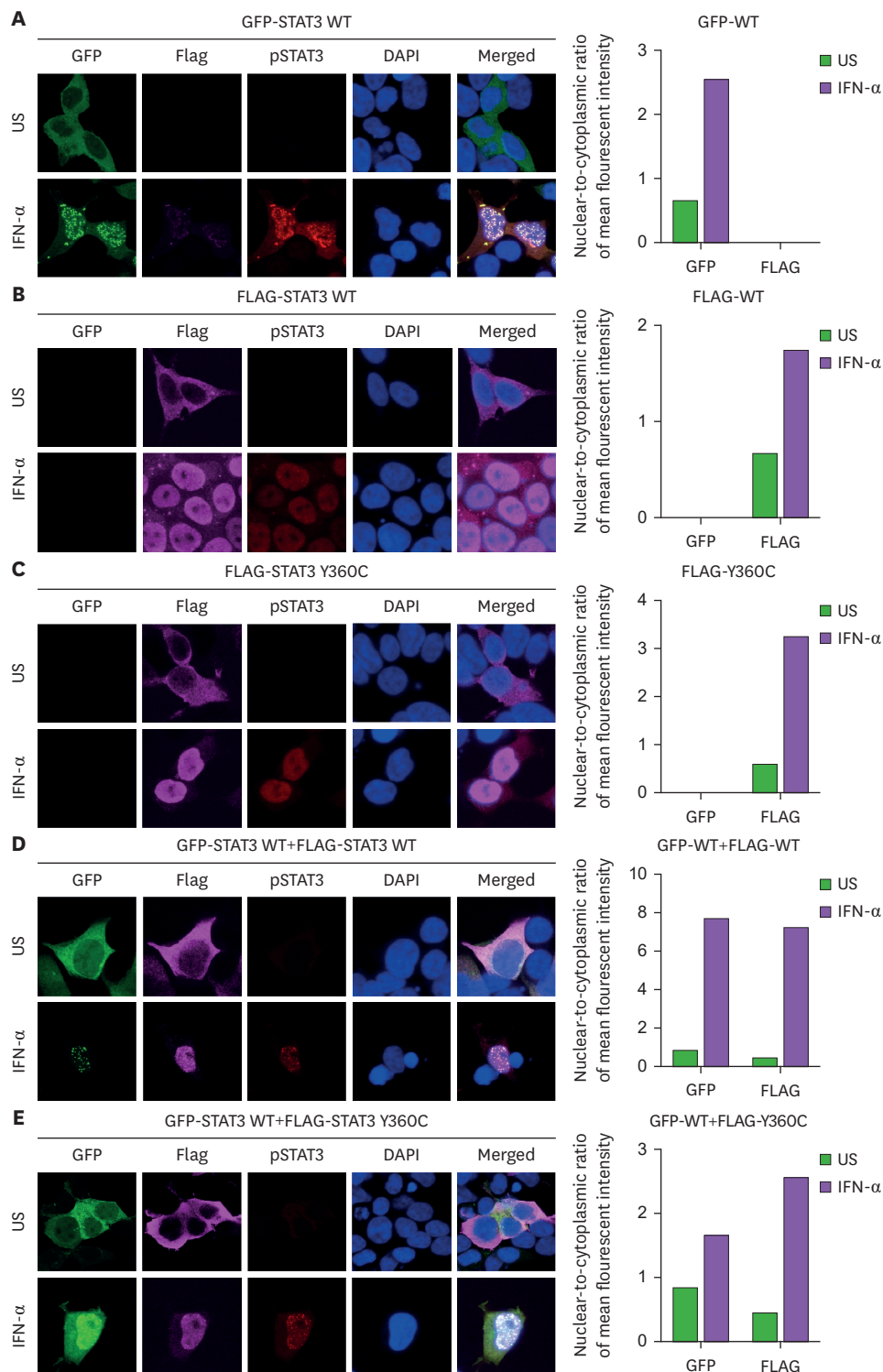


Figure 3. Immunofluorescence images of HEK293 cells expressing (A) STAT3 WT (GFP-tagged), (B) STAT3 WT (FLAG-tagged), (C) STAT3 Y360C (FLAG-tagged), co-expressing, (D) STAT3 WT (GFP-tagged and FLAG-tagged), or co-expressing, (E) STAT3 WT (GFP-tagged) and STAT3 Y360C (FLAG-tagged). Representative images from confocal microscopy (63× magnification) of total STAT3 and pSTAT3 are depicted after 30 min of IFN-α stimulation or without stimulation. Nuclear-to-cytoplasmic ratio of mean fluorescent intensity for each condition were plotted in bar charts. US, unstimulated.

STAT3 Y360C was mostly translocated to the nucleus (**Fig. 3E**, lower row). This suggests that STAT3 Y360C may have a higher efficiency than STAT3 WT in migrating to the nucleus.

STAT3 Y360C exhibits increased DNA-binding and transcriptional efficacy

To investigate the functional effects of STAT3 Y360C variants in greater detail, we established HEK293 cells that stably overexpressed STAT3 Y360C or STAT3 WT. Monoclonal cells were established from polyclonal pools of stably transduced cells via the dilution method. Intracellular staining for STAT3 followed by flow cytometry was used to detect cell clones for WT and Y360C, respectively, that expressed equivalent levels of STAT3. Since the Y360C variant is located within the DNA binding domain, we assessed its DNA binding capacity using an EMSA. Nuclear extracts were prepared from monoclonal HEK293 cells. To ensure that equivalent amounts of pSTAT3 WT and Y360C were used in this approach, nuclear lysates were first analyzed via western blot analyses (data not shown) before performing EMSA experiments. In the unstimulated condition, no DNA binding activity was detected for both STAT3 WT and STAT3 Y360C variant (**Fig. 4A**). STAT3 DNA binding activity was detectable following IFN- α stimulation, and the level of DNA binding appeared stronger in the nuclear extracts from HEK293 cells expressing the STAT3 Y360C compared to those expressing STAT3 WT (**Fig. 4A**).

Since the clinical and immunological features of STAT3 GOF patients are diverse, luciferase reporter assay and *SOCS3* expression level analysis are commonly used to confirm the GOF characteristic of *STAT3* variants (41-43). Here we examined *SOCS3* mRNA expression in HEK293 cells that stably overexpressed STAT3 Y360C or STAT3 WT. IL-6 or IFN- α stimulation resulted in far higher *SOCS3* mRNA induction in cells transduced with the *STAT3* variant constructs, compared to that of WT *STAT3* at 1–4 h following the stimulation (**Fig. 4B**). STAT3 activity in these cells was also determined using the SIE promoter via a dual-luciferase reporter assay. At the basal unstimulated condition, the STAT3 Y360C variant exhibited already a higher baseline level of STAT3 activity compared to STAT3 WT (**Fig. 4C**). Stimulation with IL-6 or IFN- α for up to 24 h also resulted in higher activity of STAT3 Y360C in comparison to that of STAT3 WT (**Fig. 4C**).

STAT3 Y360C variant is associated with increased mitochondrial activity in PBMCs

As STAT3 also exerts a function in mitochondria, we performed bioenergetics characterization evaluating mitochondrial respiration and glycolytic activity in PBMCs from patients and healthy controls using a Seahorse XF24 Extracellular Flux Analyzer. PBMCs derived from patients with *STAT3* Y360C variant displayed enhanced basal mitochondrial respiration as indicated by an elevated basal OCR in comparison to control PBMCs (**Fig. 5A**: indicated by (1) and **Fig. 5B**: indicated by (1)). Respiration linked to ATP production (ATP-linked respiration), as measured after administration of the ATP-synthase inhibitor oligomycin, was also elevated (**Fig. 5A**: indicated by (2) and **Fig. 5B**: indicated by (2)), suggesting that patients PBMCs allocate higher oxygen consumption for ATP synthesis than PBMCs from healthy controls (50). Maximal respiration measured after administration of FCCP uncouplers (**Fig. 5A**: indicated by (3) and **Fig. 5B**: indicated by (3)) and the reserve respiratory capacity (**Fig. 5A**: indicated by (4), **Fig. 5B**: indicated by (4)) were also elevated in PBMCs from the patients, demonstrating a larger contribution of mitochondria to the bioenergetics layout of Y360C STAT3. No difference in proton leakage and non-mitochondrial respiration was observed between PBMCs from patients and healthy controls (**Fig. 5A**: indicated by (5) and (6)). PBMCs harboring the *STAT3* Y360C variant exhibited a marginally

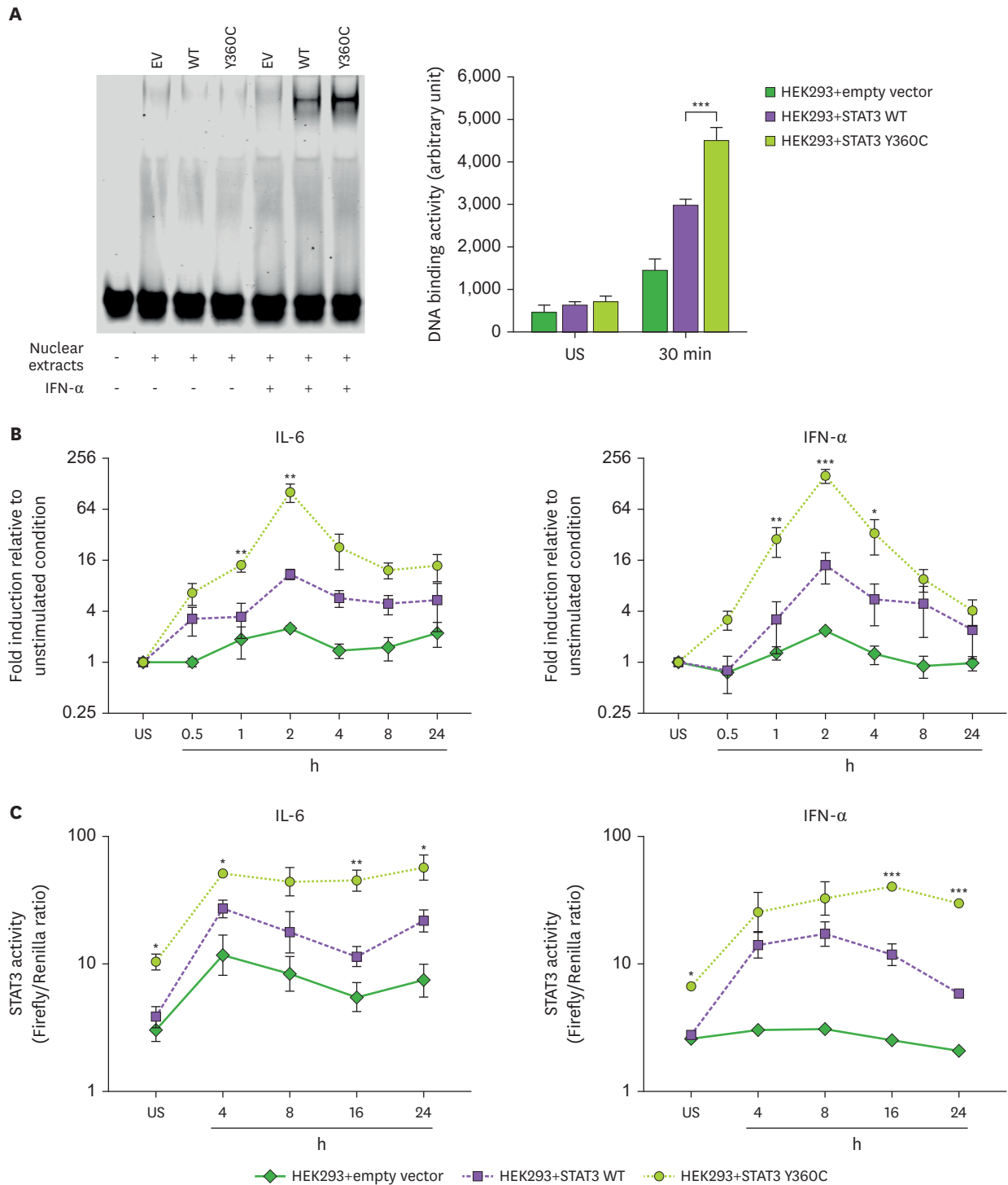


Figure 4. STAT3 Y360C variant displays increased DNA-binding capacity. Transduced HEK293 cells containing WT or Y360C STAT3 constructs were stimulated with IL-6 or IFN- α . (A) EMSA on nuclear extracts from HEK293 cells expressing either WT STAT3 or a Y360C STAT3 variant, after stimulation with IFN- α . The right panel is the quantification of 3 independent experiments. (B) mRNA expression level of *SOCS3* was determined by quantitative RT-PCR and normalized to the housekeeping gene *GAPDH*. Fold change in mRNA level as compared to the unstimulated situation is depicted. (C) STAT3 activity was determined by the luciferase reporter assay under the control of a SIE promoter. STAT3 activity was calculated by the Firefly to Renilla ratio and depicted on a log scale. All experiments were performed 3 times independently, and pooled data are shown as mean \pm SEM. Statistical analysis was performed using 2-way ANOVA followed by Šidák's multiple comparisons test.

Significant differences between WT and Y360C STAT3 constructs are demonstrated as follows: * $p < 0.05$; ** $p < 0.01$; *** $p < 0.001$.

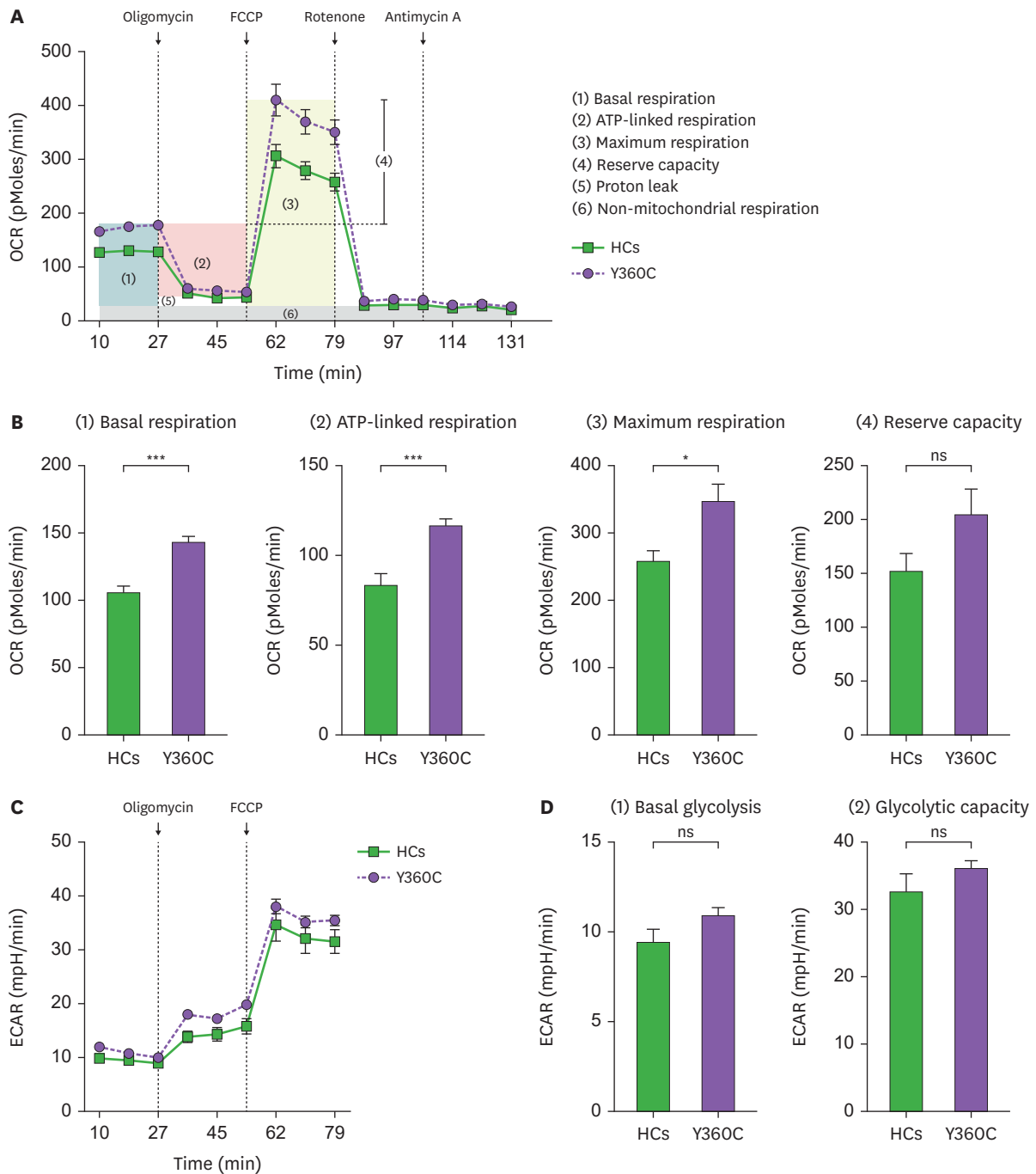


Figure 5. Mitochondrial respiration in PBMCs of patients and HCs. (A, B) OCR profile in PBMCs of both patients and HCs. PBMCs were sequentially challenged with: oligomycin for ATP synthase inhibition; the uncoupler FCCP to induce maximal respiration; rotenone and antimycin to inhibit complex I and complex III respectively, and thereby block the electron transport chain and thus respiration. The OCR profile generated 4 parameters: OCR basal respiration (1); ATP-linked respiration (2); maximum respiration (3); and reserve capacity (4). (C, D) ECAR profile in the PBMCs of patients and HCs, as measured under resting conditions and following the sequential administering of oligomycin and FCCP. The ECAR profile generated 2 parameters: basal glycolysis (1); and glycolytic capacity (2). All experiments were performed 6 times independently and data are expressed as the mean \pm SEM. Statistical analysis was performed using unpaired t-test. HC, healthy control; ns, not significant.

Significant differences are demonstrated as follows: * $p < 0.05$; *** $p < 0.001$.

elevated ECAR under basal conditions, indicating increased lactate production and enhanced glycolysis, compared to healthy controls. However, this difference was not statistically significant (**Fig. 5C** and **Fig. 5D**: indicated by (1)). Collectively, the OCR/ECAR ratio in basal conditions indicated a shift towards enhanced mitochondrial respiration in the PBMCs with the *STAT3* Y360C variant. PBMCs from the patients with the *STAT3* Y360C variant also displayed fractionally higher glycolytic capacity activity when compared to PBMCs from the healthy controls, although this was not statistically significant (**Fig. 5C** and **Fig. 5D**: indicated by (2)).

DISCUSSION

GOF variants of *STAT3* were found to be associated with severe immune dysregulation. However, the clinical presentations of such patients are divergent and the disease mechanisms underlying these clinical presentations remain unclear. The current study investigated a novel germline variant of *STAT3* located in the DNA binding domain and discovered that this variant displayed multiple immunological features associated with *STAT3* GOF syndrome. To elucidate the pathological mechanisms of the *STAT3* Y360C variant, immunological profiles, the *STAT* phosphorylation status, cytokine-induced localization of *STAT3*, DNA-binding activity, *STAT3* transcriptional activity, and mitochondrial activity were investigated.

Elevated serum levels of IL-6, IL-17A, and IL-17F were observed in several patients harboring *STAT3* GOF variants, which correlated with increased frequencies of Th17 lymphocytes (48). The differentiation of Th17 lymphocytes is primarily induced by the exposure of naïve CD4⁺ T lymphocytes to TGF- β in combination with IL-6 and IL-21, while IL-6 by itself does not promote Th17 development, as a mono-stimulator (51,52). However, in the absence of proinflammatory cytokines, TGF- β directs the differentiation of naïve T lymphocytes into Treg (52). In our study, we detected higher frequencies of Th17 lymphocytes, although this increase was not considerable. This was associated with elevated serum levels of IL-6 and IL-17 and may be considered as potential drivers of autoimmune complications in these patients with *STAT3* GOF variants. Contrary to our expectations, we did not observe a reduction in Treg frequencies. However, a comprehensive report on *STAT3* GOF syndrome indicated that Treg cell percentages were reduced in only 39% of patients, while IL-17-producing T cells were enhanced in 27%. Therefore, these parameters do not assist in the diagnosis of this disease (39).

To examine the influence of *STAT3* Y360C variant on various cellular effects, we first measured *STAT* phosphorylations. Cytokine-induced *STAT3* phosphorylation did not differ between the T lymphocytes of patients and healthy controls. This observation aligns with previous findings in other patients with GOF and LOF variants of *STAT3*, particularly when the variant is located further away from the tyrosine 705 phosphorylation site (41,46,53-55). Given that interactions between *STAT3* and other members of the *STAT* family have been documented, such interactions may influence the functioning of the immune system as well as other organ systems, potentially contributing to comorbidities observed in patients carrying the *STAT3* GOF variant (39,41,45,46). Consequently, we investigated the phosphorylation of *STAT1* and *STAT5* in T lymphocytes. In patients with the *STAT3* Y360C variant, T lymphocytes exhibited a mark reduction in *STAT1* phosphorylation upon IFN- α stimulation. Clinical and cellular phenotypic similarities of patients with *STAT1* GOF and *STAT3* LOF variants suggest that the mechanisms underlying *STAT1* and *STAT3* activities may oppose each other (56). In both *STAT1* GOF and *STAT3* LOF patients, hyperphosphorylation of *STAT1* is accompanied by increased expression of PD-L1 and decreased expression of SOCS3 (56). Overexpression of

SOCS3 has been shown to prevent IL-27-induced STAT1 hyperphosphorylation and PD-L1 expression in CD4⁺ T lymphocytes of patients with *STAT1* GOF or *STAT3* LOF variants (56). Here, we observed that Y360C *STAT3* variant displayed significantly higher levels of *SOCS3* mRNA expression following IL-6 or IFN- α stimulation compared to WT *STAT3*. This enhanced *SOCS3* expression in cells with *STAT3* GOF variants may underlie the reduced IFN- α -induced phosphorylation of STAT1, resulting in increased susceptibility to viral infections observed in these patients. Notably, this may also underpin the impairment of IFN- α -induced STAT1 signaling typically seen in patients carrying the *STAT1* LOF variant, who are predisposed to viral infections (57).

We also observed that T lymphocytes from individuals carrying the *STAT3* Y360C variant failed to phosphorylate STAT5 upon IL-2 activation. STAT5 is a crucial downstream signaling molecule of the GH receptor, and postnatal growth failure is a major characteristic of patients with the *STAT5B* LOF variant (58). Remarkably, patients carrying the *STAT3* Y360C variant displayed postnatal growth defects, suggesting that GH-induced STAT5 is likely compromised in these patients. Reduction of pSTAT5 may also be associated with increased SOCS3 activity, similar to the reduced phosphorylation of STAT1 (41).

Microscopic examination of HEK293 cells transduced with both WT and Y360C *STAT3* constructs allowed us to study cellular mechanisms that mimic the heterozygous state. This approach provided insights into how the presence of both WT and mutant *STAT3* might interact within the same cellular environment. Interestingly, following IFN- α stimulation, we observed that WT pSTAT3 in heterozygous *STAT3* Y360C HEK293 cells exhibited cytoplasmic retention. This behavior contrasts with the complete nuclear localization seen in cells expressing only WT *STAT3*. This suggests that the Y360C *STAT3* variant exhibits higher nuclear translocation efficiency and may potentially compete with the WT *STAT3* for nuclear migration. The precise mechanisms by which the Y360C variant affects the subcellular localization of WT *STAT3* remain unclear. This effect could be attributed to structural and biochemical changes resulting from cysteine substitution, leading to the introduction of a sulfhydryl group. This group can undergo oxidation, leading to the formation of disulfide bonds that stabilize *STAT3* dimers which may potentially enhance nuclear translocation (59). Notably, a study on the heterozygous *STAT5B* LOF variant in the coiled-coil domain found that the variant had a nuclear localization defect. Additionally, when dimerized with WT *STAT5B*, the variant prevented the WT from entering the nucleus (60).

Protein-nucleic acid interaction was evaluated using EMSA, revealing that the Y360C *STAT3* variant was associated with increased DNA-binding affinity, which could result in enhanced transcriptional activity detected in luciferase reporter assay and *SOCS3* mRNA expression. These findings are likely linked to alterations in the *STAT3* DBD where the variant is localized. This substitution introduces a more hydrophobic residue, potentially increasing protein-DNA interactions by stabilizing the binding interface (61). Furthermore, disulfide bond formation contributed to *STAT3* stabilization may influence its conformation and DNA-binding properties (62). These modifications might also result in prolonged nuclear localization and enhanced transcriptional activity.

Given the identification of *STAT3* in mitochondrial function, our study also focused on investigating mitochondrial activity in PBMCs from these patients. The results from patient PBMCs demonstrated that these samples exhibit significantly higher mitochondrial activity compared to controls, as evidenced by elevated basal respiration, ATP-linked respiration,

maximal respiration, and reserve respiratory capacity. Additionally, there was a marginal increase in ECAR, possibly indicating a shift towards enhanced glycolytic activity. These findings suggest that the *STAT3* Y360C GOF variant led to a hyperactive mitochondrial state, which could contribute to altered immune cell function and potentially impact the overall immune response. When stimulated by an infection, increased mitochondrial activity could provide more energy needed for immune cells to rapidly proliferate, differentiate, and perform their effector functions like phagocytosis, cytokine production, and reactive oxygen species production. However, excessive ROS production due to high mitochondrial activity could lead to oxidative stress and tissue damage as well (63,64). Supporting the result of our investigation, a study demonstrated that CD4⁺ T cells from older adults exhibit heightened basal and maximal OCRs, indicating a reliance on mitochondrial oxidative phosphorylation (29). This metabolic state was associated with increased production of proinflammatory Th17 cytokines. In contrast, activated T cells from younger, lean adults showed higher glycolytic activity. Interestingly, investigations utilizing immunoprecipitation and mass spectrometry revealed that STAT3 can form a complex with leucine-rich pentatricopeptide repeat containing protein and SLIRP in the mitochondrial matrix. This protein complex was related to lung tumorigenesis, with the DNA-binding domain of STAT3 being crucial for this interaction (65).

In conclusion, we identified a novel activating variant of STAT3. Patients with this variant exhibit a range of immune-related clinical phenotypes. Extensive biological studies revealed GOF phenotypes, including enhanced nuclear migration, increased DNA-binding capacity, and elevated STAT3 transcriptional activity. The differential phosphorylation of other STAT family members may also have contributed to the clinical manifestations in these patients. The immunometabolic profiles associated with these variants provide deeper insights into the biological functions of STAT3 and may help identify new therapeutic targets. Further studies are necessary to expand our understanding of STAT3, which will enhance the ability to diagnose and effectively treat patients with *STAT3* GOF syndrome.

ACKNOWLEDGEMENTS

The work in this manuscript has been supported by Office of the Permanent Secretary, Ministry of Higher Education, Science, Research and Innovation (OPS MHESI), Thailand Science Research and Innovation (TSRI) (Grant No. RGNS 64-002), the NSRF via the Program Management Unit for Human Resources & Institutional Development, Research and Innovation (Grant No. B16F640154), Rachadapisek Sompote Matching Fund (RA-MF-04/68), Rachadapisek Sompote Matching Fund (RA-MF-07/66), Faculty of Medicine, Chulalongkorn University, National Research Council of Thailand (NRCT) and Chulalongkorn University (N42A680063), Stichting Sophia Kinderziekenhuis Fonds (Grant No. S15-07). Erasmus MC, University Medical Center Rotterdam, the Netherlands, and the China Scholarship Council for funding PhD fellowships (No. 201908440363 Z.Z).

SUPPLEMENTARY MATERIAL

Supplementary Figure 1

Immunofluorescence images of HEK293 cells expressing STAT3 WT and STAT3 Y360C. Representative images from immunofluorescence microscopy (20× magnification) of total STAT3 and pSTAT3 are depicted after 30 min of IFN- α stimulation or without stimulation.

REFERENCES

1. Villarino AV, Kanno Y, O'Shea JJ. Mechanisms and consequences of Jak-STAT signaling in the immune system. *Nat Immunol* 2017;18:374-384. [PUBMED](#) | [CROSSREF](#)
2. Resemann HK, Watson CJ, Lloyd-Lewis B. The Stat3 paradox: a killer and an oncogene. *Mol Cell Endocrinol* 2014;382:603-611. [PUBMED](#) | [CROSSREF](#)
3. Dauer DJ, Ferraro B, Song L, Yu B, Mora L, Buettner R, Enkemann S, Jove R, Haura EB. Stat3 regulates genes common to both wound healing and cancer. *Oncogene* 2005;24:3397-3408. [PUBMED](#) | [CROSSREF](#)
4. Johnston PA, Grandis JR. STAT3 signaling: anticancer strategies and challenges. *Mol Interv* 2011;11:18-26. [PUBMED](#) | [CROSSREF](#)
5. Mali SB. Review of STAT3 (signal transducers and activators of transcription) in head and neck cancer. *Oral Oncol* 2015;51:565-569. [PUBMED](#) | [CROSSREF](#)
6. Forbes LR, Milner J, Haddad E. Signal transducer and activator of transcription 3: a year in review. *Curr Opin Hematol* 2016;23:23-27. [PUBMED](#) | [CROSSREF](#)
7. Vogel TP, Milner JD, Cooper MA. The ying and yang of STAT3 in human disease. *J Clin Immunol* 2015;35:615-623. [PUBMED](#) | [CROSSREF](#)
8. Aggarwal BB, Kunnumakkara AB, Harikumar KB, Gupta SR, Tharakan ST, Koca C, Dey S, Sung B. Signal transducer and activator of transcription-3, inflammation, and cancer: how intimate is the relationship? *Ann N Y Acad Sci* 2009;1171:59-76. [PUBMED](#) | [CROSSREF](#)
9. Jarnicki A, Putoczki T, Ernst M. Stat3: linking inflammation to epithelial cancer - more than a "gut" feeling? *Cell Div* 2010;5:14. [PUBMED](#) | [CROSSREF](#)
10. Kitamura H, Ohno Y, Toyoshima Y, Ohtake J, Homma S, Kawamura H, Takahashi N, Taketomi A. Interleukin-6/STAT3 signaling as a promising target to improve the efficacy of cancer immunotherapy. *Cancer Sci* 2017;108:1947-1952. [PUBMED](#) | [CROSSREF](#)
11. Heinrich PC, Behrmann I, Müller-Newen G, Schaper F, Graeve L. Interleukin-6-type cytokine signalling through the gp130/Jak/STAT pathway. *Biochem J* 1998;334:297-314. [PUBMED](#) | [CROSSREF](#)
12. Siveen KS, Sikka S, Surana R, Dai X, Zhang J, Kumar AP, Tan BK, Sethi G, Bishayee A. Targeting the STAT3 signaling pathway in cancer: role of synthetic and natural inhibitors. *Biochim Biophys Acta* 2014;1845:136-154. [PUBMED](#) | [CROSSREF](#)
13. Delgoffe GM, Vignali DA. STAT heterodimers in immunity: a mixed message or a unique signal? *JAKSTAT* 2013;2:e23060. [PUBMED](#) | [CROSSREF](#)
14. Nkansah E, Shah R, Collie GW, Parkinson GN, Palmer J, Rahman KM, Bui TT, Drake AF, Husby J, Neidle S, et al. Observation of unphosphorylated STAT3 core protein binding to target dsDNA by PEMS and X-ray crystallography. *FEBS Lett* 2013;587:833-839. [PUBMED](#) | [CROSSREF](#)
15. Liu L, McBride KM, Reich NC. STAT3 nuclear import is independent of tyrosine phosphorylation and mediated by importin- α 3. *Proc Natl Acad Sci U S A* 2005;102:8150-8155. [PUBMED](#) | [CROSSREF](#)
16. Yang J, Liao X, Agarwal MK, Barnes L, Auron PE, Stark GR. Unphosphorylated STAT3 accumulates in response to IL-6 and activates transcription by binding to NF κ B. *Genes Dev* 2007;21:1396-1408. [PUBMED](#) | [CROSSREF](#)
17. Timofeeva OA, Chasovskikh S, Lonskaya I, Tarasova NI, Khavrutskii L, Tarasov SG, Zhang X, Korostyshevskiy VR, Cheema A, Zhang L, et al. Mechanisms of unphosphorylated STAT3 transcription factor binding to DNA. *J Biol Chem* 2012;287:14192-14200. [PUBMED](#) | [CROSSREF](#)
18. Hillmer EJ, Zhang H, Li HS, Watowich SS. STAT3 signaling in immunity. *Cytokine Growth Factor Rev* 2016;31:1-15. [PUBMED](#) | [CROSSREF](#)
19. Toth KA, Schmitt EG, Kolichesk A, Greenberg ZJ, Levendosky E, Saucier N, Trammel K, Oikonomou V, Lionakis MS, Klechevsky E, et al. A human STAT3 gain-of-function variant drives local Th17 dysregulation and skin inflammation in mice. *J Exp Med* 2024;221:e20232091. [PUBMED](#) | [CROSSREF](#)
20. Carow B, Rottenberg ME. SOCS3, a major regulator of infection and inflammation. *Front Immunol* 2014;5:58. [PUBMED](#) | [CROSSREF](#)
21. Rottenberg ME, Carow B. SOCS3 and STAT3, major controllers of the outcome of infection with *Mycobacterium tuberculosis*. *Semin Immunol* 2014;26:518-532. [PUBMED](#) | [CROSSREF](#)
22. Gao Y, Zhao H, Wang P, Wang J, Zou L. The roles of SOCS3 and STAT3 in bacterial infection and inflammatory diseases. *Scand J Immunol* 2018;88:e12727. [PUBMED](#) | [CROSSREF](#)
23. Sobah ML, Liongue C, Ward AC. SOCS proteins in immunity, inflammatory diseases, and immune-related cancer. *Front Med (Lausanne)* 2021;8:727987. [PUBMED](#) | [CROSSREF](#)
24. Yang R, Rincon M. Mitochondrial Stat3, the need for design thinking. *Int J Biol Sci* 2016;12:532-544. [PUBMED](#) | [CROSSREF](#)

25. Wegrzyn J, Potla R, Chwae YJ, Sepuri NB, Zhang Q, Koeck T, Derecka M, Szczepanek K, Szlag M, Gornicka A, et al. Function of mitochondrial Stat3 in cellular respiration. *Science* 2009;323:793-797. [PUBMED](#) | [CROSSREF](#)
26. Gough DJ, Corlett A, Schlessinger K, Wegrzyn J, Larner AC, Levy DE. Mitochondrial STAT3 supports Ras-dependent oncogenic transformation. *Science* 2009;324:1713-1716. [PUBMED](#) | [CROSSREF](#)
27. Rincon M, Pereira FV. A new perspective: mitochondrial stat3 as a regulator for lymphocyte function. *Int J Mol Sci* 2018;19:1656. [PUBMED](#) | [CROSSREF](#)
28. Yang R, Lirussi D, Thornton TM, Jelley-Gibbs DM, Diehl SA, Case LK, et al. Mitochondrial Ca²⁺ and membrane potential, an alternative pathway for interleukin 6 to regulate CD4 cell effector function. *Elife* 2015;4:e06376. [PUBMED](#) | [CROSSREF](#)
29. Zukowski E, Sannella M, Rockhold JD, Kalantar GH, Yu J, SantaCruz-Calvo S, Kuhn MK, Hah N, Ouyang L, Wang TW, et al. STAT3 modulates CD4⁺ T mitochondrial dynamics and function in aging. *Aging Cell* 2023;22:e13996. [PUBMED](#) | [CROSSREF](#)
30. Holland SM, DeLeo FR, Elloumi HZ, Hsu AP, Uzel G, Brodsky N, Freeman AF, Demidowich A, Davis J, Turner ML, et al. STAT3 mutations in the hyper-IgE syndrome. *N Engl J Med* 2007;357:1608-1619. [PUBMED](#) | [CROSSREF](#)
31. Buckley RH. The hyper-IgE syndrome. *Clin Rev Allergy Immunol* 2001;20:139-154. [PUBMED](#) | [CROSSREF](#)
32. Tsilifis C, Freeman AF, Gennery AR. STAT3 hyper-IgE syndrome-an update and unanswered questions. *J Clin Immunol* 2021;41:864-880. [PUBMED](#) | [CROSSREF](#)
33. Milner JD, Brechley JM, Laurence A, Freeman AF, Hill BJ, Elias KM, Kanno Y, Spalding C, Elloumi HZ, Paulson ML, et al. Impaired T_H17 cell differentiation in subjects with autosomal dominant hyper-IgE syndrome. *Nature* 2008;452:773-776. [PUBMED](#) | [CROSSREF](#)
34. Minegishi Y, Saito M, Nagasawa M, Takada H, Hara T, Tsuchiya S, Agematsu K, Yamada M, Kawamura N, Ariga T, et al. Molecular explanation for the contradiction between systemic Th17 defect and localized bacterial infection in hyper-IgE syndrome. *J Exp Med* 2009;206:1291-1301. [PUBMED](#) | [CROSSREF](#)
35. de Beaucoudrey L, Puel A, Filipe-Santos O, Cobat A, Ghandil P, Chrabieh M, Feinberg J, von Bernuth H, Samarina A, Jannière L, et al. Mutations in STAT3 and IL12RB1 impair the development of human IL-17-producing T cells. *J Exp Med* 2008;205:1543-1550. [PUBMED](#) | [CROSSREF](#)
36. Wu J, Chen J, Tian ZQ, Zhang H, Gong RL, Chen TX, Hong L. Clinical manifestations and genetic analysis of 17 patients with autosomal dominant hyper-IgE syndrome in Mainland China: new reports and a literature review. *J Clin Immunol* 2017;37:166-179. [PUBMED](#) | [CROSSREF](#)
37. Bergerson JRE, Freeman AF. An update on syndromes with a hyper-IgE phenotype. *Immunol Allergy Clin North Am* 2019;39:49-61. [PUBMED](#) | [CROSSREF](#)
38. Fabre A, Marchal S, Barlogis V, Mari B, Barbry P, Rohrlisch PS, Forbes LR, Vogel TP, Giovannini-Chami L. Clinical aspects of STAT3 gain-of-function germline mutations: a systematic review. *J Allergy Clin Immunol Pract* 2019;7:1958-1969.e9. [PUBMED](#) | [CROSSREF](#)
39. Leiding JW, Vogel TP, Santarlas VGJ, Mhaskar R, Smith MR, Carisey A, Vargas-Hernández A, Silva-Carmona M, Heeg M, Rensing-Ehl A, et al. Monogenic early-onset lymphoproliferation and autoimmunity: natural history of STAT3 gain-of-function syndrome. *J Allergy Clin Immunol* 2023;151:1081-1095. [PUBMED](#) | [CROSSREF](#)
40. Haddad E. STAT3: too much may be worse than not enough! *Blood* 2015;125:583-584. [PUBMED](#) | [CROSSREF](#)
41. Milner JD, Vogel TP, Forbes L, Ma CA, Stray-Pedersen A, Niemela JE, Lyons JJ, Engelhardt KR, Zhang Y, Topcagic N, et al. Early-onset lymphoproliferation and autoimmunity caused by germline STAT3 gain-of-function mutations. *Blood* 2015;125:591-599. [PUBMED](#) | [CROSSREF](#)
42. Haapaniemi EM, Kaustio M, Rajala HL, van Adrichem AJ, Kainulainen L, Glumoff V, Doffinger R, Kuusanmäki H, Heiskanen-Kosma T, Trotta L, et al. Autoimmunity, hypogammaglobulinemia, lymphoproliferation, and mycobacterial disease in patients with activating mutations in STAT3. *Blood* 2015;125:639-648. [PUBMED](#) | [CROSSREF](#)
43. Flanagan SE, Haapaniemi E, Russell MA, Caswell R, Allen HL, De Franco E, McDonald TJ, Rajala H, Ramelius A, Barton J, et al. Activating germline mutations in STAT3 cause early-onset multi-organ autoimmune disease. *Nat Genet* 2014;46:812-814. [PUBMED](#) | [CROSSREF](#)
44. Velayos T, Martínez R, Alonso M, Garcia-Etxebarria K, Aguayo A, Camarero C, Urrutia I, Martínez de LaPiscina I, Barrio R, Santin I, et al. An activating mutation in STAT3 results in neonatal diabetes through reduced insulin synthesis. *Diabetes* 2017;66:1022-1029. [PUBMED](#) | [CROSSREF](#)
45. Sediva H, Dusatkova P, Kanderova V, Obermannova B, Kayserova J, Sramkova L, Zemkova D, Elblova L, Svaton M, Zachova R, et al. Short stature in a boy with multiple early-onset autoimmune conditions due to a STAT3 activating mutation: could intracellular growth hormone signalling be compromised?. *Horm Res Paediatr* 2017;88:160-166. [PUBMED](#) | [CROSSREF](#)

46. Gutiérrez M, Scaglia P, Keselman A, Martucci L, Karabatas L, Domené S, Martin A, Pennisi P, Blanco M, Sanguinetti N, et al. Partial growth hormone insensitivity and dysregulatory immune disease associated with de novo germline activating STAT3 mutations. *Mol Cell Endocrinol* 2018;473:166-177. [PUBMED](#) | [CROSSREF](#)
47. Milanese C, Cerri S, Ulusoy A, Gornati SV, Plat A, Gabriels S, Blandini F, Di Monte DA, Hoeijmakers JH, Mastroberardino PG. Activation of the DNA damage response in vivo in synucleinopathy models of Parkinson's disease. *Cell Death Dis* 2018;9:818. [PUBMED](#) | [CROSSREF](#)
48. Wienke J, Janssen W, Scholman R, Spits H, van Gijn M, Boes M, van Montfrans J, Moes N, de Roock S. A novel human STAT3 mutation presents with autoimmunity involving Th17 hyperactivation. *Oncotarget* 2015;6:20037-20042. [PUBMED](#) | [CROSSREF](#)
49. Meesilpavikkai K, Dik WA, Schrijver B, Nagtzaam NM, van Rijswijk A, Driessen GJ, van der Spek PJ, van Hagen PM, Dalm VA. A novel heterozygous mutation in the STAT1 SH2 domain causes chronic mucocutaneous candidiasis, atypically diverse infections, autoimmunity, and impaired cytokine regulation. *Front Immunol* 2017;8:274. [PUBMED](#) | [CROSSREF](#)
50. Brand MD, Nicholls DG. Assessing mitochondrial dysfunction in cells. *Biochem J* 2011;435:297-312. [PUBMED](#) | [CROSSREF](#)
51. Mangan PR, Harrington LE, O'Quinn DB, Helms WS, Bullard DC, Elson CO, Hatton RD, Wahl SM, Schoeb TR, Weaver CT. Transforming growth factor-beta induces development of the T_H17 lineage. *Nature* 2006;441:231-234. [PUBMED](#) | [CROSSREF](#)
52. Lee GR. The balance of Th17 versus Treg cells in autoimmunity. *Int J Mol Sci* 2018;19:730. [PUBMED](#) | [CROSSREF](#)
53. Renner ED, Rylaarsdam S, Anover-Sombke S, Rack AL, Reichenbach J, Carey JC, Zhu Q, Jansson AF, Barboza J, Schimke LF, et al. Novel signal transducer and activator of transcription 3 (STAT3) mutations, reduced T_H17 cell numbers, and variably defective STAT3 phosphorylation in hyper-IgE syndrome. *J Allergy Clin Immunol* 2008;122:181-187. [PUBMED](#) | [CROSSREF](#)
54. Minegishi Y, Saito M, Tsuchiya S, Tsuge I, Takada H, Hara T, Kawamura N, Ariga T, Pasic S, Stojkovic O, et al. Dominant-negative mutations in the DNA-binding domain of STAT3 cause hyper-IgE syndrome. *Nature* 2007;448:1058-1062. [PUBMED](#) | [CROSSREF](#)
55. Pelham SJ, Lenthall HC, Deenick EK, Tangye SG. Elucidating the effects of disease-causing mutations on STAT3 function in autosomal-dominant hyper-IgE syndrome. *J Allergy Clin Immunol* 2016;138:1210-1213.e5. [PUBMED](#) | [CROSSREF](#)
56. Zhang Y, Ma CA, Lawrence MG, Break TJ, O'Connell MP, Lyons JJ, López DB, Barber JS, Zhao Y, Barber DL, et al. PD-L1 up-regulation restrains Th17 cell differentiation in STAT3 loss- and STAT1 gain-of-function patients. *J Exp Med* 2017;214:2523-2533. [PUBMED](#) | [CROSSREF](#)
57. Casanova JL, Holland SM, Notarangelo LD. Inborn errors of human JAKs and STATs. *Immunity* 2012;36:515-528. [PUBMED](#) | [CROSSREF](#)
58. Hwa V. STAT5B deficiency: impacts on human growth and immunity. *Growth Horm IGF Res* 2016;28:16-20. [PUBMED](#) | [CROSSREF](#)
59. Cremers CM, Jakob U. Oxidant sensing by reversible disulfide bond formation. *J Biol Chem* 2013;288:26489-26496. [PUBMED](#) | [CROSSREF](#)
60. Klammt J, Neumann D, Gevers EF, Andrew SF, Schwartz ID, Rockstroh D, Colombo R, Sanchez MA, Vokurkova D, Kowalczyk J, et al. Dominant-negative STAT5B mutations cause growth hormone insensitivity with short stature and mild immune dysregulation. *Nat Commun* 2018;9:2105. [PUBMED](#) | [CROSSREF](#)
61. Yesudhas D, Batool M, Anwar MA, Panneerselvam S, Choi S. Proteins recognizing DNA: structural uniqueness and versatility of DNA-binding domains in stem cell transcription factors. *Genes (Basel)* 2017;8:192. [PUBMED](#) | [CROSSREF](#)
62. Kalodimos CG, Folkers GE, Boelens R, Kaptein R. Strong DNA binding by covalently linked dimeric Lac headpiece: evidence for the crucial role of the hinge helices. *Proc Natl Acad Sci U S A* 2001;98:6039-6044. [PUBMED](#) | [CROSSREF](#)
63. Faas MM, de Vos P. Mitochondrial function in immune cells in health and disease. *Biochim Biophys Acta Mol Basis Dis* 2020;1866:165845. [PUBMED](#) | [CROSSREF](#)
64. Wang Y, Li N, Zhang X, Horng T. Mitochondrial metabolism regulates macrophage biology. *J Biol Chem* 2021;297:100904. [PUBMED](#) | [CROSSREF](#)
65. Fernando CD, Jayasekara WSN, Inampudi C, Kohonen-Corish MRJ, Cooper WA, Beilharz TH, Josephs TM, Garama DJ, Gough DJ. A STAT3 protein complex required for mitochondrial mRNA stability and cancer. *Cell Rep* 2023;42:113033. [PUBMED](#) | [CROSSREF](#)